Supplementary Information

A computational study of CO_2 hydrogenation on single atoms of Pt, Pd, Ni and Rh adsorbed on $In_2O_3(111)$

Francesco Cannizzaro, Sjoerd Kurstjens, Tom van den Berg, and Emiel J. M. Hensen* and Ivo A. W. Filot*
Laboratory of Inorganic Materials and Catalysis, Department of Chemistry and Chemical Engineering, Eindhoven University of Technology, Eindhoven, The Netherlands 5600 MB (NL)

*E-mail: E.J.M.Hensen@tue.nl

*E-mail: i.a.w.filot@tue.nl

Table of Contents

S1: Binding energies of single atoms on In_2O_3(111) 2
S2: Electronic structure analysis 4
S3: Oxygen vacancies 5
S4. Geometries of elementary reaction steps on Ni-In_2O_3(111) 6
S5. Geometries of elementary reaction steps on Pd-In_2O_3(111) 8
S6. Geometries of elementary reaction steps on Pt-In_2O_3(111) 10
S7. Geometries of elementary reaction steps on Rh-In_2O_3(111) 12
S8: Parameters for microkinetic simulations 14
S9: Microkinetic simulations 18
S10: Additional DFT calculations 21
Supporting References 22

S1: Binding energies of single atoms on $In_2O_3(111)$

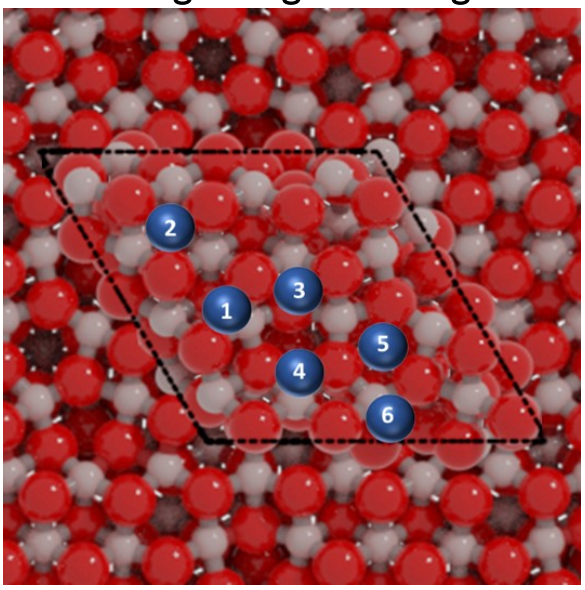

Fig. S1. Adsorption sites for single atoms on $In_2O_3(111)$. Blue: SA. Grey: In. Red: O.

Table S1. Adsorption energies (kJ/mol) of single atoms on the indicated by Fig. S1. The reference for the metal (Ni, Pd, Pt and Rh) is a single atom in the gas phase.

		E_b [kJ/mol]		
ID	**Ni**	**Pd**	**Pt**	**Rh**
1	-512	-339	-481	-355
2	-484	-328	-461	-425
3	-484	-318	-450	-401
4	-479	-311	-457	-383
5	-411	-309	-411	-346
6	-415	-305	-428	-328

Table S2. Reaction and activation energies (kJ/mol) for the migration of SA (SA = Pd, Pt, Ni and Rh) on stable adsorption sites on the In_2O_3(111) surface as shown in **Fig**.1.

	Ni-In_2O_3		**Pd-In_2O_3**		**Pt-In_2O_3**		**Rh-In_2O_3**	
ID	E_R	E_a	E_R	E_a	E_R	E_a	E_R	E_a
1 → 3	32	101	8	34	32	131	33	100
3→4	11	178	3	44	15	156	20	143
4→5	68	154	5	27	24	101	76	142

S2: Electronic structure analysis

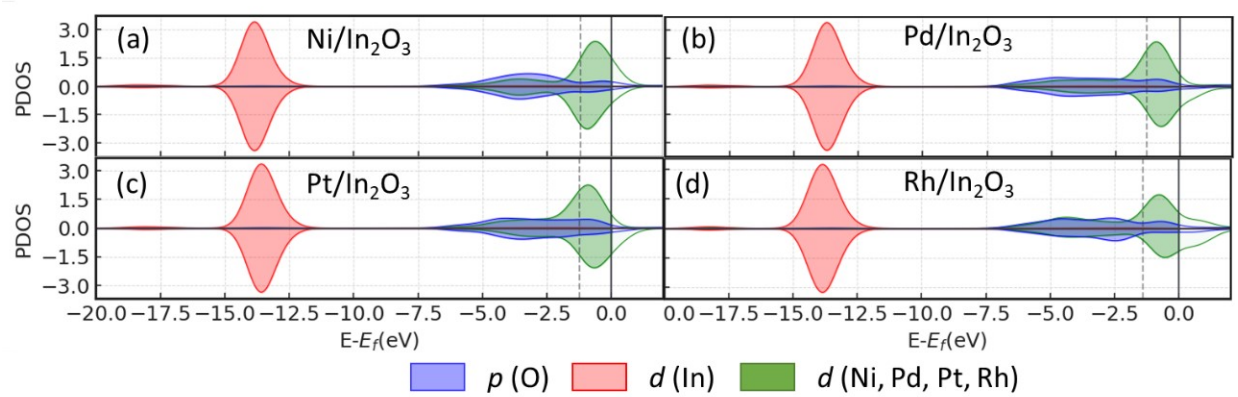

Fig. S2. Partial density of state (PDOS) of Ni 3*d*, Pd 4*d*, Pt 5*d* and Rh 4*d*, O 2*p* (the O atom adjacent to the metal SA) and In *d* orbitals. (a) Ni-In_2O_3, (b) Pd-In_2O_3, (c) Pt-In_2O_3 and (d) Rh-In_2O_3.

S3: Oxygen vacancies

Table S3. Oxygen vacancy formation energies with repsect to gas-phase H_2O (kJ/mol) for bare In_2O_3 and SA-promoted In_2O_3 surfaces.

ID	**In_2O_3**	**Ni-In_2O_3**	**Pd-In_2O_3**	**Pt-In_2O_3**	**Rh-In_2O_3**
1	-61	139	-77	54	38
2	-61	140	-22	215	39
3	-60	139	-70	-35	105
4	-51	137	29	176	62
5	-51	149	25	173	39
6	-50	154	24	146	128
7	8	161	75	210	170
8	5	190	74	210	96
9	7	161	80	217	141
10	-6	161	53	217	125
11	-5	168	52	187	124
12	-5	169	52	185	123

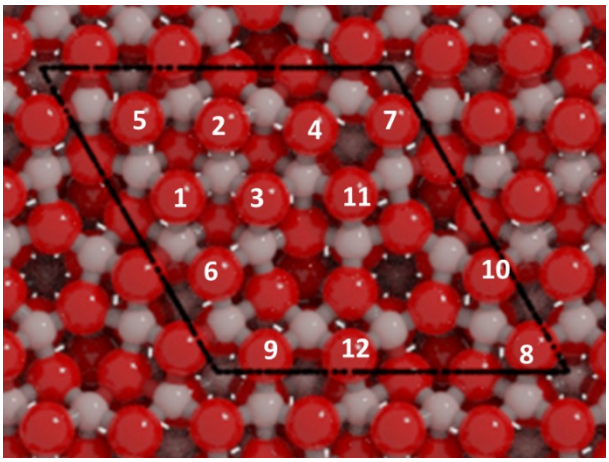

Fig. S3. Positions of the 12 surface oxygens for the calculations reported in Table S2 (red: O; grey: In).

Table S4. Geometrical parameters (Å) and oxygen vacancy formation energy ($E_{Ov,}$ in kJ/mol) for the O atom directly connected to the SA with the lowest E_{Ov}.

	Ni-In_2O_3(111)	**Pd-In_2O_3(111)**	**Pt-In_2O_3(111)**	**Rh-In_2O_3(111)**
$d_{M\text{-}O}$ / Å	1.82	2.13	2.10	1.98
E_{Ov} / kJ/mol	141	-71	-35	39

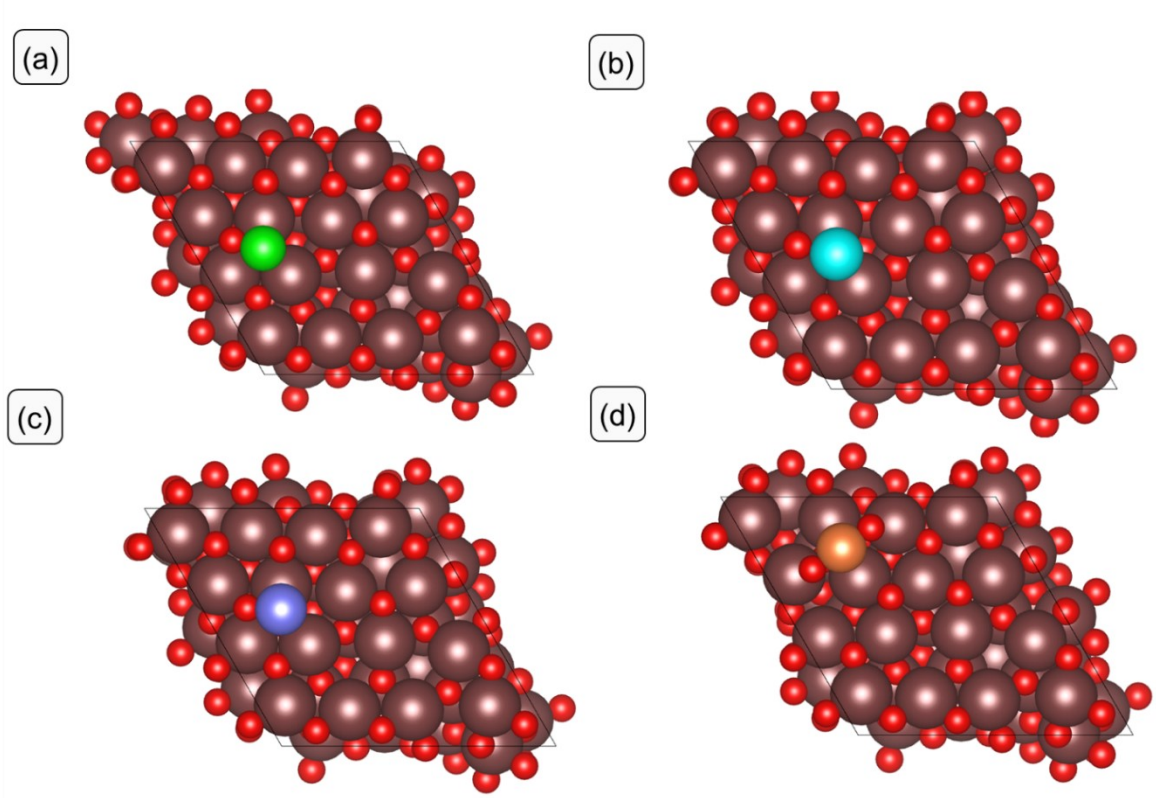

Fig. S4. Position of the SA on the In_2O_3(111) surface after formation of an oxygen vacancy. (a) Ni-, (b) Pd-, (c) Pt- and (d) Rh-In_2O_3. Brown: In, red: O, green: Ni, light blue: Pd, purple: Pt, orange: Rh.

S4. Geometries of elementary reaction steps

CO_2 adsorption

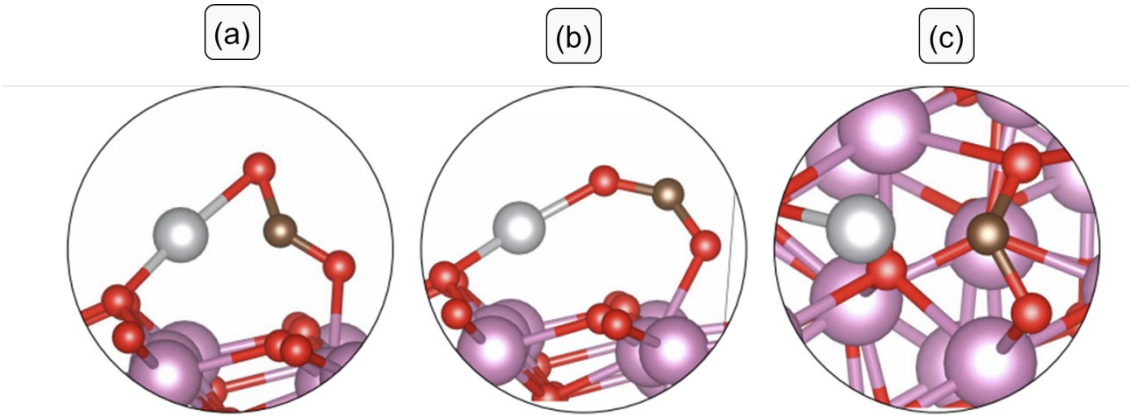

Fig. S5. Bonding configurations of CO_2 on SA-In_2O_3 models. Red: O, black: C, pink: In, grey: Ni, Pd, Pt or Rh. The most stable configuration features CO_2 adsorbed near an oxygen vacancy with both O and C close to the single metal atom. Adsorption configurations depicted in Figure S5b-c are significantly less stable.

Table S5. Adsorption energies (kJ/mol) for the configurations reported in Figure S5**.**

	E_{ads} (kJ/mol)			
	Ni-In_2O_3	**Pd-In_2O_3**	**Pt-In_2O_3**	**Rh-In_2O_3**
(a)	-144	-31	-33	-87
(b)	-44	+62	+16	-33
(c)	-34	+28	+37	-24

Table S6. Ni-In_2O_3

1. $H_2 + 2* \rightleftharpoons 2H^*$			2. $H^* + OH^* \rightleftharpoons H_2O^*$		
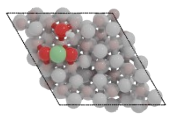	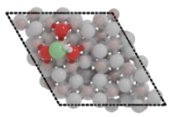	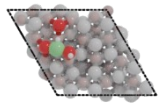	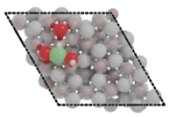	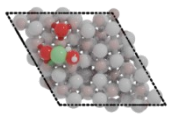	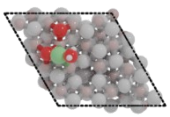
3. $H_2O + * \rightleftharpoons H_2O^*$			4. $CO_2(g) + * \rightleftharpoons CO_2^* +$		
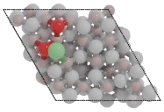		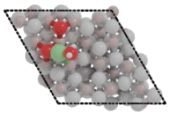	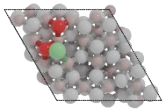		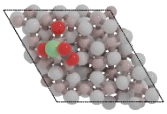
5. $CO_2^* + 2* + H_2 \rightleftharpoons CO_2^* + 2H$			6. $CO_2^* + 2H^* \rightleftharpoons HCOO^* + * + H^*$		
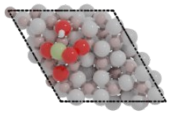	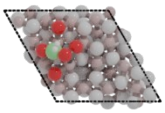	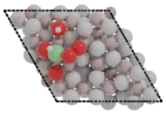	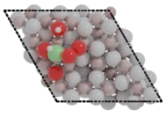	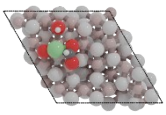	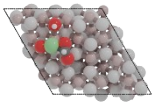
7. $HCOO^* + H^* \rightleftharpoons H_2COO^* + *$			8. $H_2COO^* \rightleftharpoons H_2CO^* + O^*$		
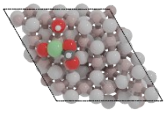	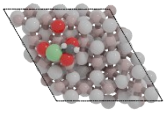	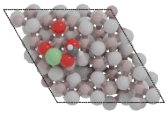	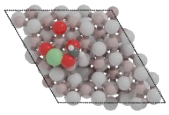	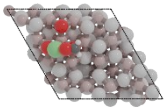	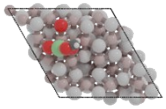
9. $CH_2O^* + H_2(g) + 2* \rightleftharpoons CH_2O^* + 2H^*$			10. $CH_2O^* + H^* \rightleftharpoons CH_3O^* + *$		
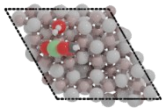	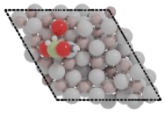	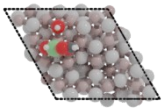	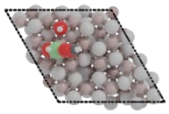	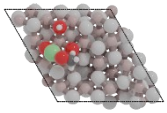	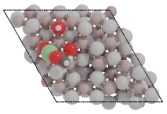
11. $CH_3O^* + H^* \rightleftharpoons CH_3OH(g) + *$					

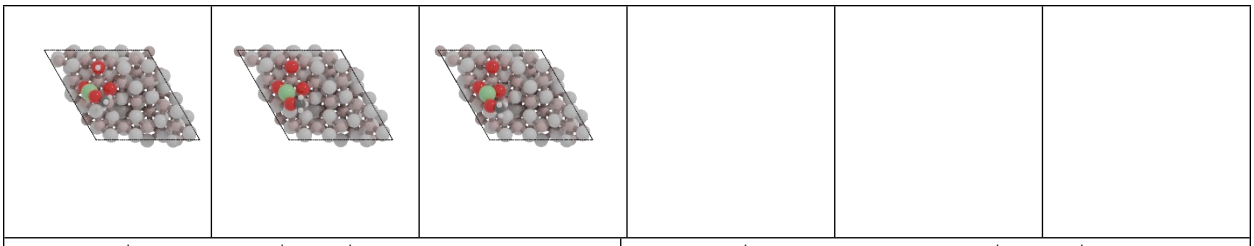

12. $CO^*{}_2 + * \rightleftharpoons CO^* + O^*$

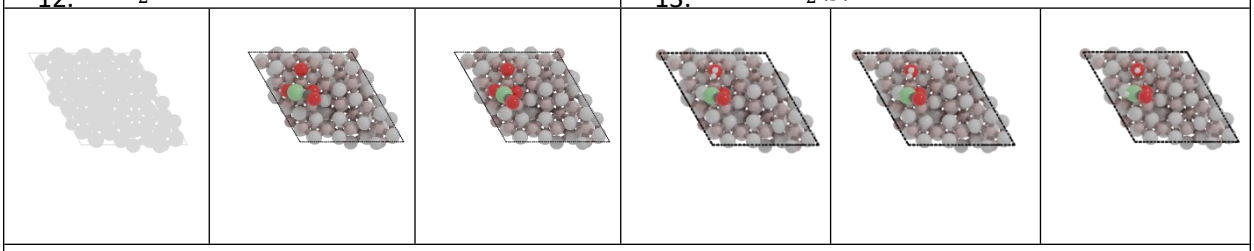

13. $CO^* + H_2(g) + 2* \rightleftharpoons CO^* + 2H^*$

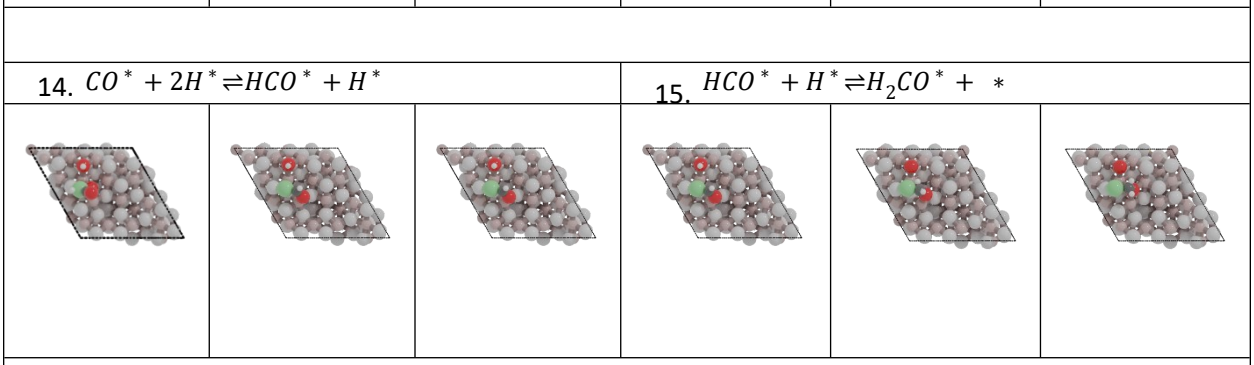

14. $CO^* + 2H^* \rightleftharpoons HCO^* + H^*$

15. $HCO^* + H^* \rightleftharpoons H_2CO^* + *$

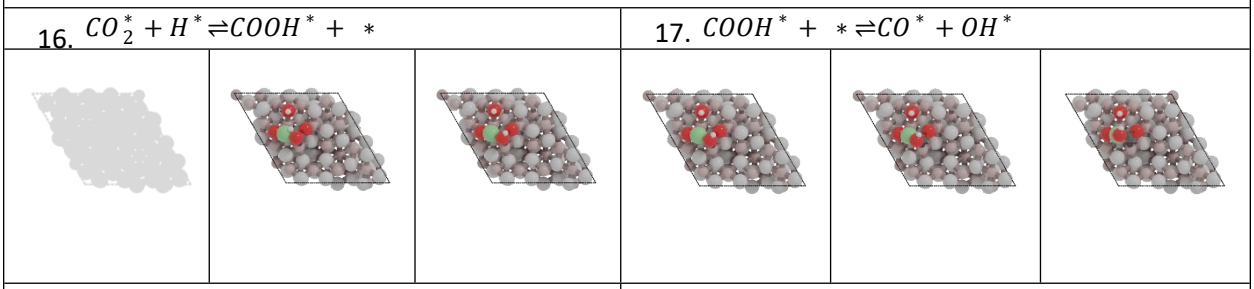

16. $CO_2^* + H^* \rightleftharpoons COOH^* + *$

17. $COOH^* + * \rightleftharpoons CO^* + OH^*$

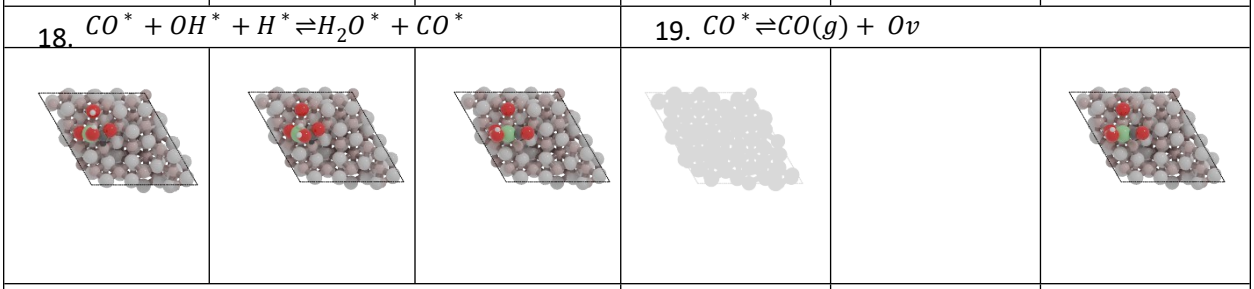

18. $CO^* + OH^* + H^* \rightleftharpoons H_2O^* + CO^*$

19. $CO^* \rightleftharpoons CO(g) + Ov$

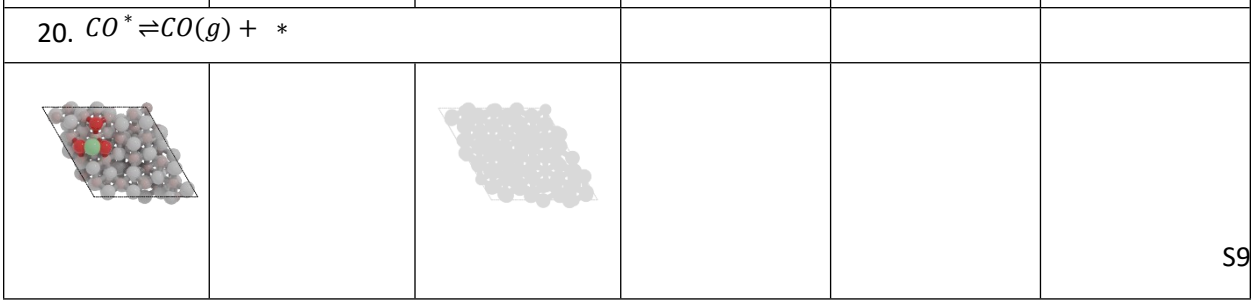

20. $CO^* \rightleftharpoons CO(g) + *$

Table S7. Pd-In_2O_3

1. $H_2 + 2* \rightleftharpoons 2H^*$			2. $H^* + OH^* \rightleftharpoons H_2O^*$		
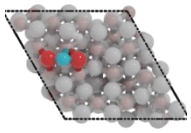	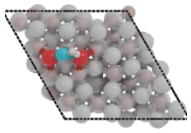	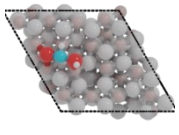	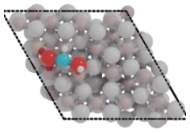	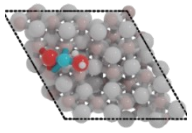	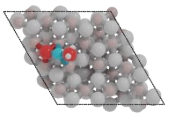
3. $H_2O + * \rightleftharpoons H_2O^*$			4. $CO_2(g) + * \rightleftharpoons CO_2^* +$		
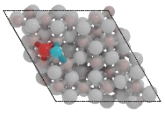		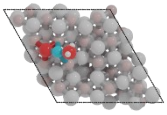	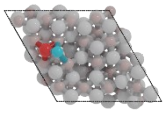		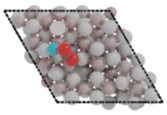
5. $CO_2^* + 2* + H_2 \rightleftharpoons CO_2^* + 2H$			6. $CO_2^* + 2H^* \rightleftharpoons HCOO^* + * + H^*$		
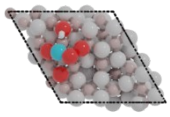	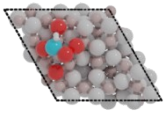	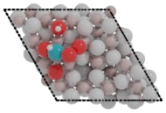	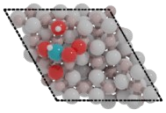	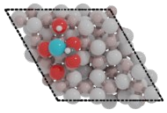	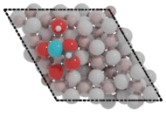
7. $HCOO^* + H^* \rightleftharpoons H_2COO^* + *$			8. $H_2COO^* \rightleftharpoons H_2CO^* + O^*$		
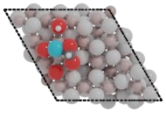	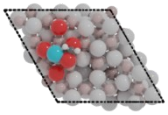	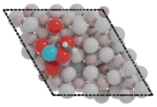	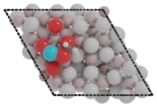	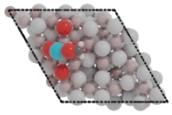	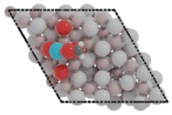
9. $CH_2O^* + H_2(g) + 2* \rightleftharpoons CH_2O^* + 2H^*$			10. $CH_2O^* + H^* \rightleftharpoons CH_3O^* + *$		
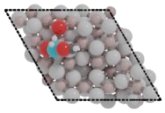	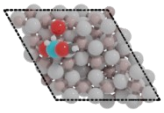	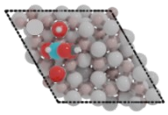	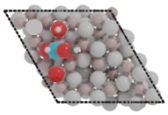	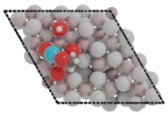	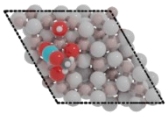
11. $CH_3O^* + H^* \rightleftharpoons CH_3OH(g) + *$					
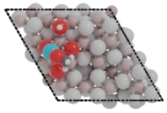	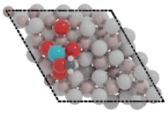	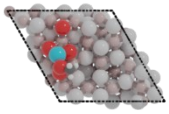			

12. $CO^*{}_2 + * \rightleftharpoons CO^* + O^*$

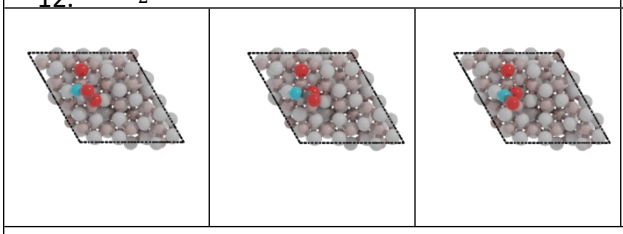

13. $CO^* + H_2(g) + 2* \rightleftharpoons CO^* + 2H^*$

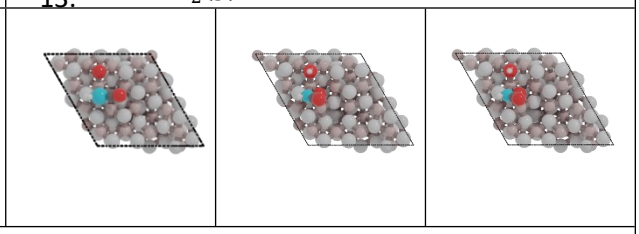

14. $CO^* + 2H^* \rightleftharpoons HCO^* + H^*$

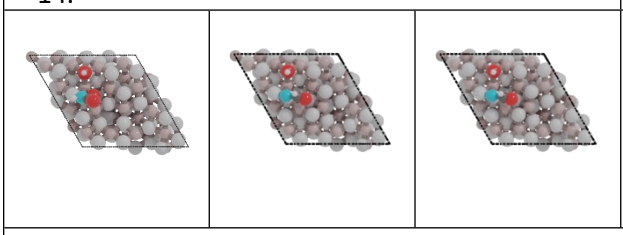

15. $HCO^* + H^* \rightleftharpoons H_2CO^* + *$

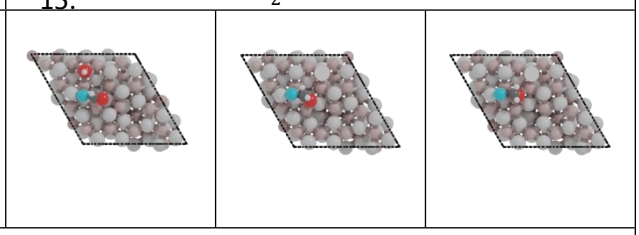

16. $CO_2^* + H^* \rightleftharpoons COOH^* + *$

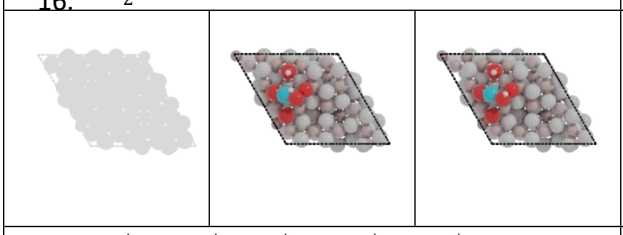

17. $COOH^* + * \rightleftharpoons CO^* + OH^*$

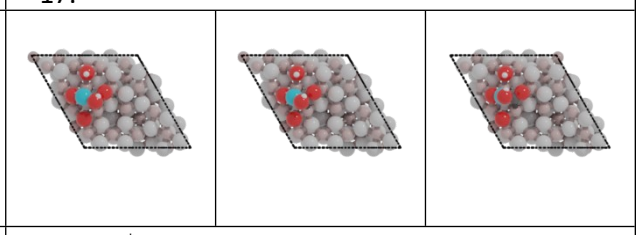

18. $CO^* + OH^* + H^* \rightleftharpoons H_2O^* + CO^*$

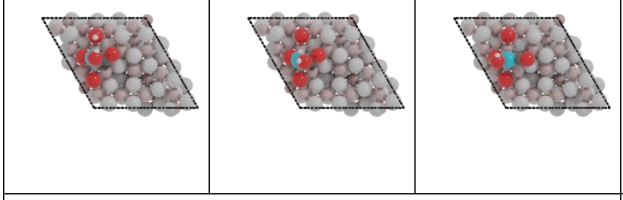

19. $CO^* \rightleftharpoons CO(g) + Ov$

20. $CO^* \rightleftharpoons CO(g) + *$

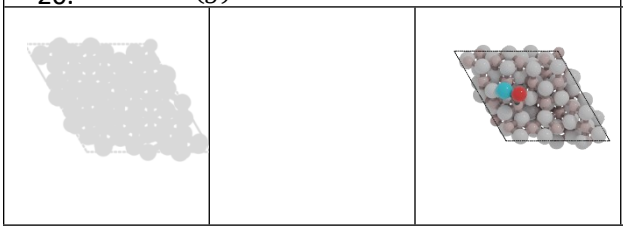

Table S8. Pt-In_2O_3

1. $H_2 + 2* \rightleftharpoons 2H^*$			2. $H^* + OH^* \rightleftharpoons H_2O^*$		
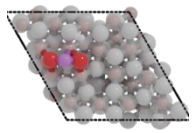	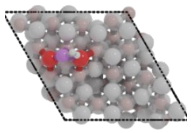	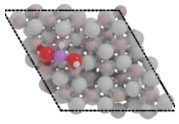	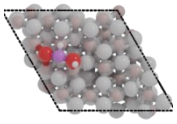	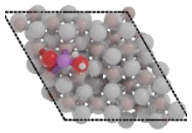	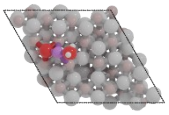
3. $H_2O + * \rightleftharpoons H_2O^*$			4. $CO_2(g) + * \rightleftharpoons CO_2^* +$		
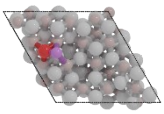		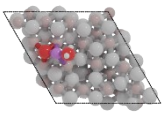	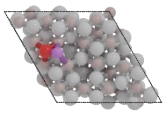		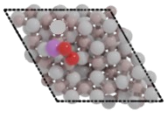
5. $CO_2^* + 2* + H_2 \rightleftharpoons CO_2^* + 2H$			6. $CO_2^* + 2H^* \rightleftharpoons HCOO^* + * + H^*$		
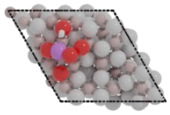	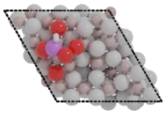	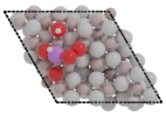	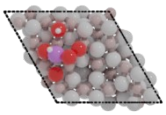	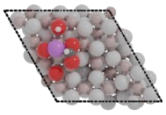	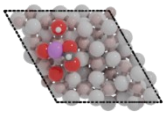
7. $HCOO^* + H^* \rightleftharpoons H_2COO^* + *$			8. $H_2COO^* \rightleftharpoons H_2CO^* + O^*$		
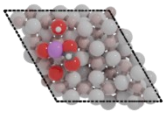	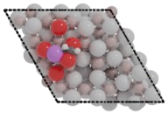	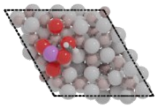	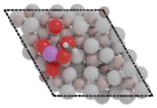	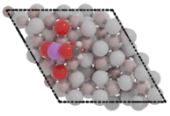	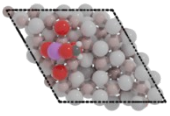
9. $CH_2O^* + H_2(g) + 2* \rightleftharpoons CH_2O^* + 2H^*$			10. $CH_2O^* + H^* \rightleftharpoons CH_3O^* + *$		
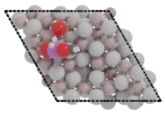	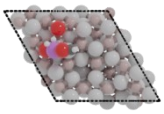	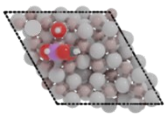	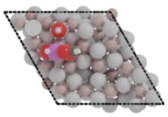	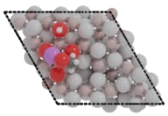	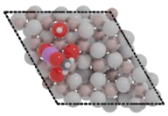
11. $CH_3O^* + H^* \rightleftharpoons CH_3OH(g) + *$					
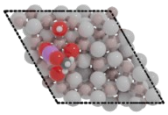	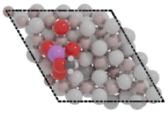	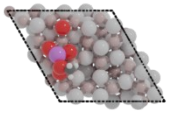			
12. $CO^*{}_2 + * \rightleftharpoons CO^* + O^*$			13.		

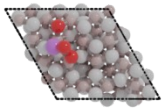	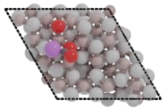	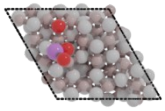	N.A.	N.A.	N.A.
14.			15.		
N.A.	N.A.	N.A.	N.A.	N.A.	N.A.
16. $CO_2^* + H^* \rightleftharpoons COOH^* + *$			17. $COOH^* + * \rightleftharpoons CO^* + OH^*$		
	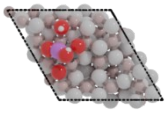	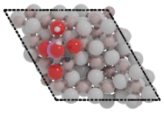	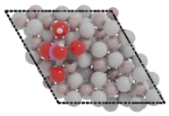	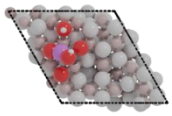	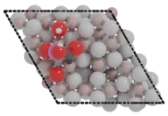
18. $CO^* + OH^* + H^* \rightleftharpoons H_2O^* + CO^*$			19. $CO^* \rightleftharpoons CO(g) + Ov$		
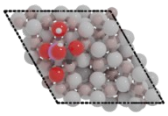	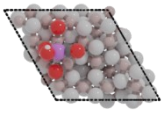	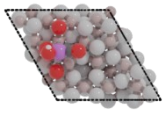			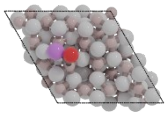
20. $CO^* \rightleftharpoons CO(g) + *$					
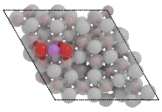		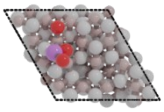			

Table S9. Rh-In_2O_3

1. $H_2 + 2* \rightleftharpoons 2H^*$			2. $H^* + OH^* \rightleftharpoons H_2O^*$		
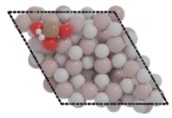	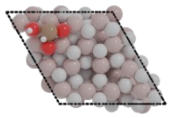	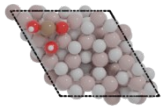	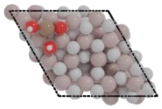	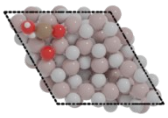	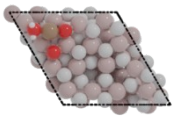
3. $H_2O + * \rightleftharpoons H_2O^*$			4. $CO_2(g) + * \rightleftharpoons CO_2^* +$		
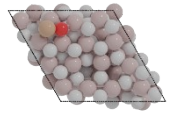		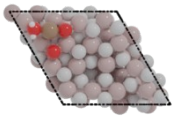	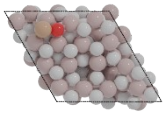		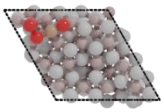
5. $CO_2^* + 2* + H_2 \rightleftharpoons CO_2^* + 2H$			6. $CO_2^* + 2H^* \rightleftharpoons HCOO^* + * + H^*$		
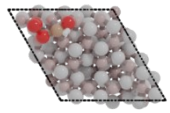	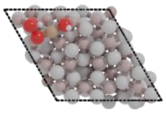	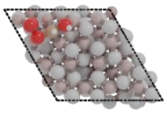	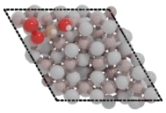	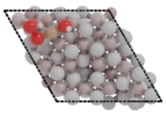	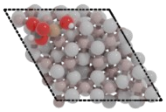
7. $HCOO^* + H^* \rightleftharpoons H_2COO^* + *$			8. $H_2COO^* \rightleftharpoons CH_2O^* + O^*$		
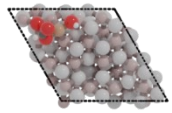	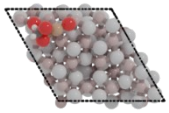	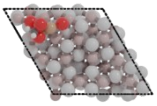	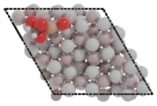	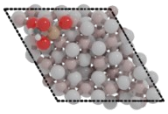	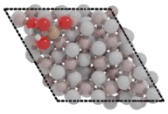
9. $CH_2O^* + H_2(g) + 2* \rightleftharpoons CH_2O^* + 2H^*$			10. $CH_2O^* + H^* \rightleftharpoons CH_3O^* + *$		
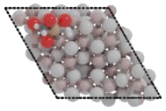	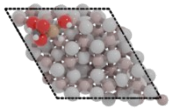	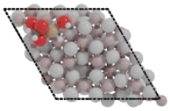	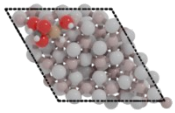	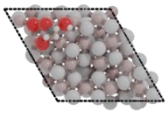	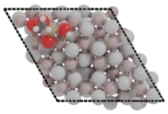
11. $CH_3O^* + H^* \rightleftharpoons CH_3OH(g) + *$					
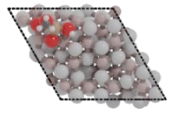	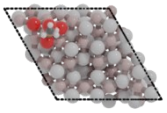	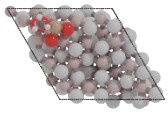			
12. $CO^*{}_2 + * \rightleftharpoons CO^* + O^*$			13. $CO^* + H_2(g) + 2* \rightleftharpoons CO^* + 2H^*$		

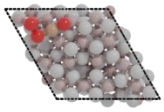	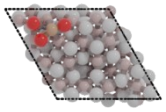	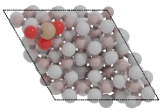	**N.A.**	**N.A.**	**N.A.**
14. $CO^* + 2H^* \rightleftharpoons HCO^* + H^*$			15. $HCO^* + H^* \rightleftharpoons H_2CO^* + *$		
N.A.	N.A.	N.A.	**N.A.**	**N.A.**	**N.A.**
16. $CO_2^* + H^* \rightleftharpoons COOH^* + *$			17. $COOH^* + * \rightleftharpoons CO^* + OH^*$		
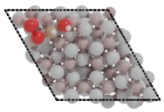	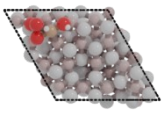	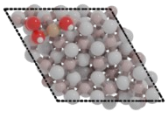	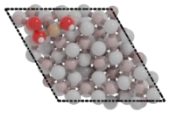	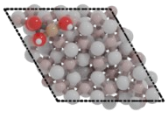	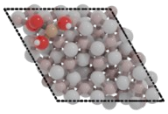
18. $CO^* + OH^* + H^* \rightleftharpoons H_2O^* + CO^*$			19. $CO^* \rightleftharpoons CO(g) + Ov$		
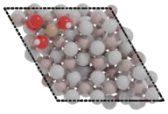	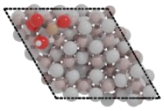	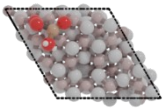			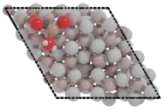
20. $CO^* \rightleftharpoons CO(g) + *$					
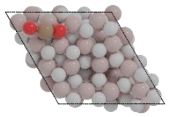		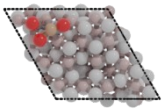			

S5: Parameters for microkinetic simulations

Table S10. Kinetic parameters including ratio of partition functions of the TS and IS (Q_{TS}/Q_{IS}) and TS and FS (Q_{TS}/Q_{FS}), forward ($E_{act,f}$) and backward ($E_{act,f}$) activation energies for CO_2 hydrogenation to CH_3OH, CO and H_2O over Ni-In_2O_3 model.

	Elementary steps	Q_{TS}/Q_{IS}	Q_{TS}/Q_{FS}	$E_{act,f}$ (kJ/mol)	$E_{act,b}$ (kJ/mol)
	Oxygen vacancy formation pathway				
1	$H_2(g) + 2* \rightleftharpoons 2H^*$	0.20	0.57	19	55
2	$H^* + OH^* \rightleftharpoons H_2O^* + O^*$	1.70	0.39	93	66
3	$H_2O^* \rightleftharpoons H_2O(g) + *$	1.0	1.0	177	-
	Formate pathway to CH_3OH				
4	$CO_2(g) + * \rightleftharpoons CO_2^*$	1.0	1.0	-	144
5	$CO_2^* + H_2(g) + 2* \rightleftharpoons CO_2^* + 2H^*$	0.20	0.57	19	55
6	$CO_2^* + 2H^* \rightleftharpoons HCO_2^* + H^* + *$	5.55	0.59	66	68
7	$HCO_2^* + H^* \rightleftharpoons H_2CO_2^* + *$	0.17	1.44	114	34
8	$H_2CO_2^* + * \rightleftharpoons CH_2O^* + O*$	1.05	0.28	101	33
9	$CH_2O^* + H_2(g) + 2* \rightleftharpoons CH_2O^* + 2H^*$	0.20	0.57	19	55
10	$CH_2O^* + 2H^* \rightleftharpoons CH_3O^* + H^*$	0.47	0.54	55	132
11	$CH_3O^* + H^* \rightleftharpoons CH_3OH_{(g)}$	0.06	0.61	61	54
	CO hydrogenation pathway to CH_3OH				
12	$CO^*{}_2 + * \rightleftharpoons CO^* + O^*$	0.52	0.17	81	78
13	$CO^* + H_2(g) + 2* \rightleftharpoons CO^* + 2H^*$	0.20	0.57	19	55
14	$CO^* + 2H^* \rightleftharpoons HCO^* + H^*$	0.52	0.17	71	65
15	$HCO^* + H^* \rightleftharpoons CH_2O^* + *$	0.20	0.57	177	35
	rWGS pathway to CO				
16	$CO^*{}_2 + 2H^* \rightleftharpoons COOH^* + H^* + *$	0.31	0.02	82	69
17	$COOH^* + * \rightleftharpoons CO^* + OH^*$	1.13	0.33	45	25
18	$CO^* + OH^* + H^* \rightleftharpoons CO^* + H_2O^*$	1.51	0.96	140	198
19	$CO^* \rightleftharpoons CO(g) + Ov$	1.0	1.0	51	-
20	$CO^* \rightleftharpoons CO(g) + *$	1.0	1.0	121	-

Activation energies (E_{act}) were directly obtained from DFT calculations. All DFT energies are corrected by the zero-point energy (ZPE). Numbers are the same as in Figure 3a.

Pre-exponential factors were estimated by transition state theory at T = 550 K.

Table S11. Kinetic parameters including ratio of partition functions of the TS and IS (Q_{TS}/Q_{IS}) and TS and FS (Q_{TS}/Q_{FS}), forward ($E_{act,f}$) and backward ($E_{act,f}$) activation energies for CO_2 hydrogenation to CH_3OH, CO and H_2O over Pd-In_2O_3 model.

	Elementary steps	Q_{TS}/Q_{IS}	Q_{TS}/Q_{FS}	$E_{act,f}$ (kJ/mol)	$E_{act,b}$ (kJ/mol)
	Oxygen vacancy formation pathway				
1	$H_2(g) + 2* \rightleftharpoons 2H^*$	0.20	0.57	62	72
2	$H^* + OH^* \rightleftharpoons H_2O^* + O^*$	1.70	0.39	47	127
3	$H_2O^* \rightleftharpoons H_2O(g) + *$	1.0	1.0	12	-
	Formate pathway to CH_3OH				
4	$CO_2(g) + * \rightleftharpoons CO_2^*$	1.0	1.0	-	31
5	$CO_2^* + H_2(g) + 2* \rightleftharpoons CO_2^* + 2H^*$	0.20	0.57	104	247
6	$CO_2^* + 2H^* \rightleftharpoons HCO_2^* + H^* + *$	5.55	0.59	40	12
7	$HCO_2^* + H^* \rightleftharpoons H_2CO_2^* + *$	0.17	1.44	220	53
8	$H_2CO_2^* + * \rightleftharpoons CH_2O^* + O^*$	1.05	0.28	62	8
9	$CH_2O^* + H_2(g) + 2* \rightleftharpoons CH_2O^* + 2H^*$	0.20	0.57	73	94
10	$CH_2O^* + 2H^* \rightleftharpoons CH_3O^* + H^*$	0.47	0.54	62	40
11	$CH_3O^* + H^* \rightleftharpoons CH_3OH_{(g)}$	0.06	0.61	106	141
	CO hydrogenation pathway to CH_3OH				
12	$CO^*{}_2 + * \rightleftharpoons CO^* + O^*$	0.52	0.17	65	91
13	$CO^* + H_2(g) + 2* \rightleftharpoons CO^* + 2H^*$	0.20	0.57	41	74
14	$CO^* + 2H^* \rightleftharpoons HCO^* + H^*$	1.0	1.0	148	55
15	$HCO^* + H^* \rightleftharpoons CH_2O^* + *$	1.0	1.0	128	14
	rWGS pathway to CO				
16	$CO^*{}_2 + 2H^* \rightleftharpoons COOH^* + H^* + *$	0.31	0.02	61	81
17	$COOH^* + * \rightleftharpoons CO^* + OH^*$	1.13	0.33	42	23
18	$CO^* + OH^* + H^* \rightleftharpoons CO^* + H_2O^*$	1.51	0.96	140	82
19	$CO^* \rightleftharpoons CO(g) + Ov$	1.0	1.0	25	-
20	$CO^* \rightleftharpoons CO(g) + *$	1.0	1.0	31	-

Activation energies (E_{act}) were directly obtained from DFT calculations. All DFT energies are corrected by the zero-point energy (ZPE). Numbers are the same as in Figure 3b.

Pre-exponential factors were estimated by transition state theory at T = 550 K.

Table S12. Kinetic parameters including ratio of partition functions of the TS and IS (Q_{TS}/Q_{IS}) and TS and FS (Q_{TS}/Q_{FS}), forward ($E_{act,f}$) and backward ($E_{act,f}$) activation energies for CO_2 hydrogenation to CH_3OH, CO and H_2O over Pt-In_2O_3 model.

	Elementary steps	Q_{TS}/Q_{IS}	Q_{TS}/Q_{FS}	$E_{act,f}$ (kJ/mol)	$E_{act,b}$ (kJ/mol)
	Oxygen vacancy formation pathway				
1	$H_2(g) + 2* \rightleftharpoons 2H^*$	0.20	0.57	48	144
2	$H^* + OH^* \rightleftharpoons H_2O^* + O^*$	1.70	0.39	68	48
3	$H_2O^* \rightleftharpoons H_2O(g) + *$	1.0	1.0	41	-
	Formate pathway to CH_3OH				
4	$CO_2(g) + * \rightleftharpoons CO_2^*$	1.0	1.0	-	31
5	$CO_2^* + H_2(g) + 2* \rightleftharpoons CO_2^* + 2H^*$	0.20	0.57	48	142
6	$CO_2^* + 2H^* \rightleftharpoons HCO_2^* + H^* + *$	5.55	0.59	34	66
7	$HCO_2^* + H^* \rightleftharpoons H_2CO_2^* + *$	0.17	1.44	146	17
8	$H_2CO_2^* + * \rightleftharpoons CH_2O^* + O*$	1.05	0.28	156	56
9	$CH_2O^* + H_2(g) + 2* \rightleftharpoons CH_2O^* + 2H^*$	0.20	0.57	23	203
10	$CH_2O^* + 2H^* \rightleftharpoons CH_3O^* + H^*$	0.47	0.54	80	65
11	$CH_3O^* + H^* \rightleftharpoons CH_3OH_{(g)}$	0.06	0.61	118	105
	rWGS pathway to CO				
12	$CO^*_2 + * \rightleftharpoons CO^* + O^*$	0.52	0.17	65	91
16	$CO^*_2 + 2H^* \rightleftharpoons COOH^* + H^* + *$	0.31	0.02	147	92
17	$COOH^* + * \rightleftharpoons CO^* + OH^*$	1.13	0.33	65	32
18	$CO^* + OH^* + H^* \rightleftharpoons CO^* + H_2O^*$	1.51	0.96	133	149
19	$CO^* \rightleftharpoons CO(g) + Ov$	1.0	1.0	24	-
20	$CO^* \rightleftharpoons CO(g) + *$	1.0	1.0	158	-

Activation energies (E_{act}) were directly obtained from DFT calculations. All DFT energies are corrected by the zero-point energy (ZPE).Numbers are the same as in Figure 3c.

Pre-exponential factors were estimated by transition state theory at T = 550 K.

Table S13. Kinetic parameters including ratio of partition functions of the TS and IS (Q_{TS}/Q_{IS}) and TS and FS (Q_{TS}/Q_{FS}), forward ($E_{act,f}$) and backward ($E_{act,f}$) activation energies for CO_2 hydrogenation to CH_3OH, CO and H_2O over Rh-In_2O_3 model.

	Elementary steps	Q_{TS}/Q_{IS}	Q_{TS}/Q_{FS}	$E_{act,f}$ (kJ/mol)	$E_{act,b}$ (kJ/mol)
	Oxygen vacancy formation pathway				
1	$H_2(g) + 2* \rightleftharpoons 2H^*$	0.20	0.57	57	201
2	$H^* + OH^* \rightleftharpoons H_2O^* + O^*$	1.70	0.39	76	7
3	$H_2O^* \rightleftharpoons H_2O(g) + *$	1.0	1.0	26	-
	Formate pathway to CH_3OH				
4	$CO_2(g) + * \rightleftharpoons CO_2^*$	1.0	1.0	-	87
5	$CO_2^* + H_2(g) + 2* \rightleftharpoons CO_2^* + 2H^*$	0.20	0.57	51	85
6	$CO_2^* + 2H^* \rightleftharpoons HCO_2^* + H^* + *$	5.55	0.59	42	95
7	$HCO_2^* + H^* \rightleftharpoons H_2CO_2^* + *$	0.17	1.44	155	19
8	$H_2CO_2^* + * \rightleftharpoons CH_2O^* + O*$	1.05	0.28	101	34
9	$CH_2O^* + H_2(g) + 2* \rightleftharpoons CH_2O^* + 2H^*$	0.20	0.57	25	209
10	$CH_2O^* + 2H^* \rightleftharpoons CH_3O^* + H^*$	0.47	0.54	149	133
11	$CH_3O^* + H^* \rightleftharpoons CH_3OH_{(g)}$	0.06	0.61	135	119
	rWGS pathway to CO				
12	$CO^*{}_2 + * \rightleftharpoons CO^* + O^*$	0.52	0.17	80	78
16	$CO^*{}_2 + 2H^* \rightleftharpoons COOH^* + H^* + *$	0.31	0.02	59	138
17	$COOH^* + * \rightleftharpoons CO^* + OH^*$	1.13	0.33	25	45
18	$CO^* + OH^* + H^* \rightleftharpoons CO^* + H_2O^*$	1.51	0.96	186	68
19	$CO^* \rightleftharpoons CO(g) + Ov$	1.0	1.0	120	-
20	$CO^* \rightleftharpoons CO(g) + *$	1.0	1.0	215	-

Activation energies (E_{act}) were directly obtained from DFT calculations. All DFT energies are corrected by the zero-point energy (ZPE).Numbers are the same as in Figure 3d.

Pre-exponential factors were estimated by transition state theory at *T* = 550 K.

S9: Further Microkinetic simulations

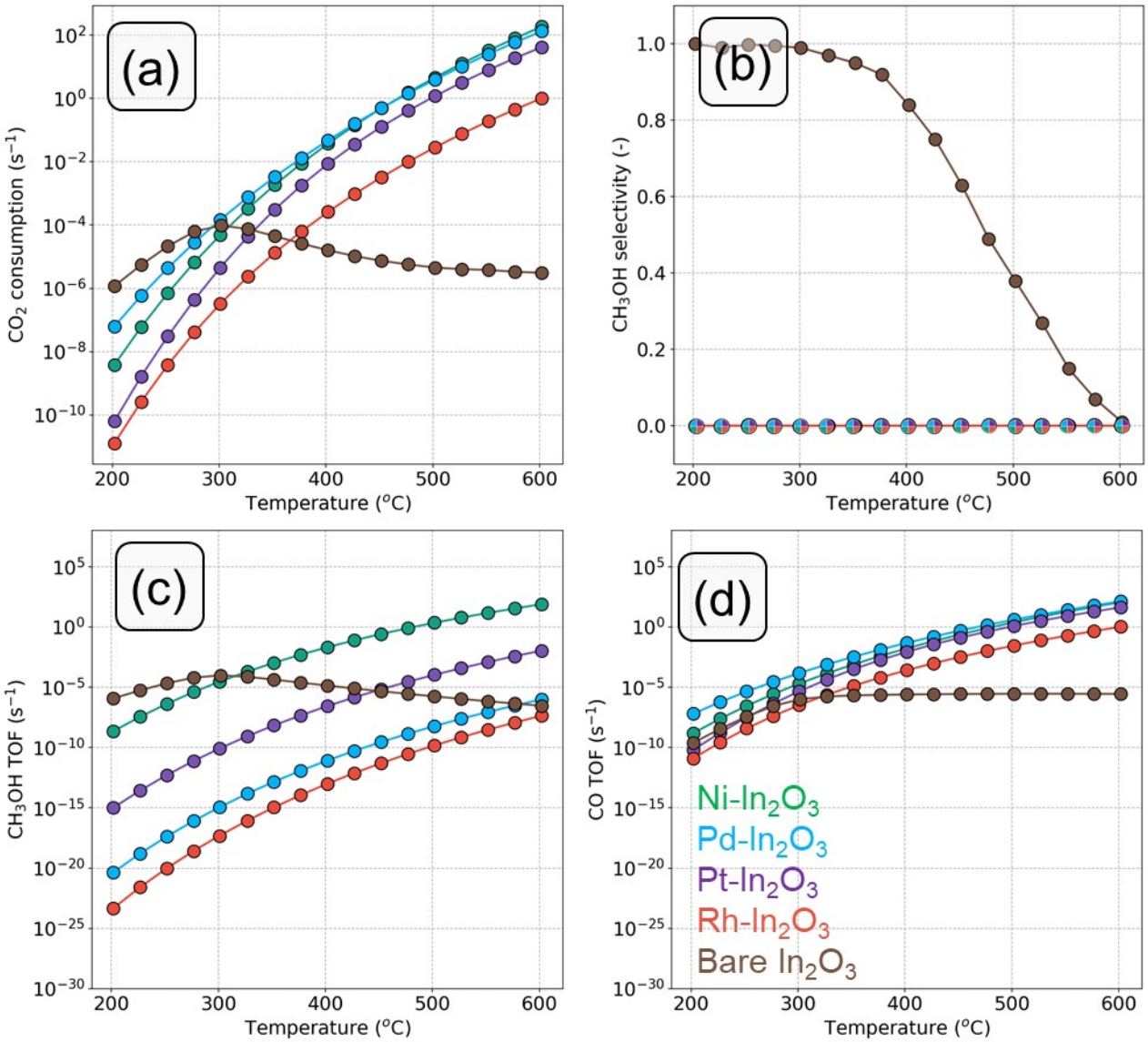

Fig. S6: (a) CO_2 consumption rate (s^{-1}), (b) CH_3OH selectivity, (c) CH_3OH TOF (s^{-1}) and (d) CO TOF in s^{-1} as a function of temperature on SA-In_2O_3 models (p = 50 bar, H_2/CO_2 ratio =5). The data for In_2O_3-bare are taken from reference [1]

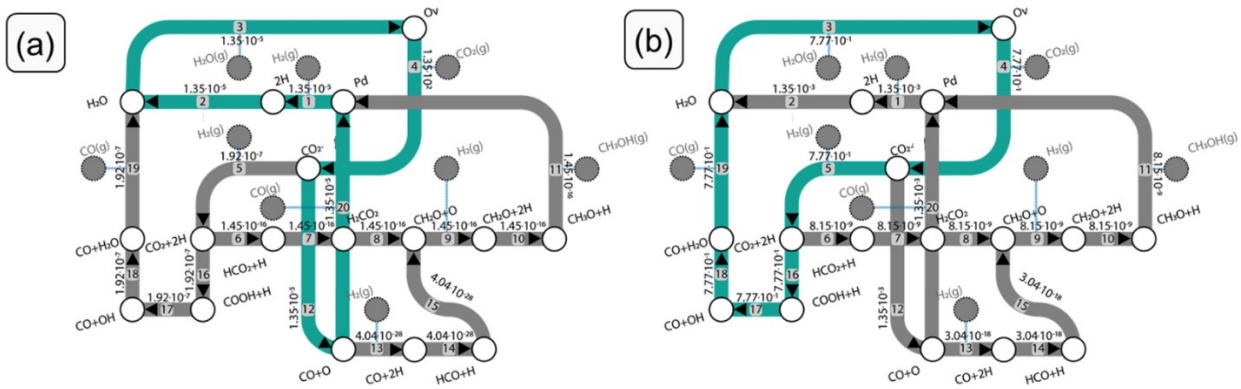

Fig. S7. Molar fluxes analysis for Pd-In_2O_3. (a) T = 200 °C and (b) T = 450 °C. The dominant pathway for each model is indicated by the colored pathways.

Table S14. Binding energies of SA-O (SA = Ni, Pd, Pt and Rh) and In-O in kJ/mol taken from ref[2].

	E_b [kJ/mol]
Ni-O	391
Rh-O	377
In-O	360
Pt-O	347
Pd-O	234

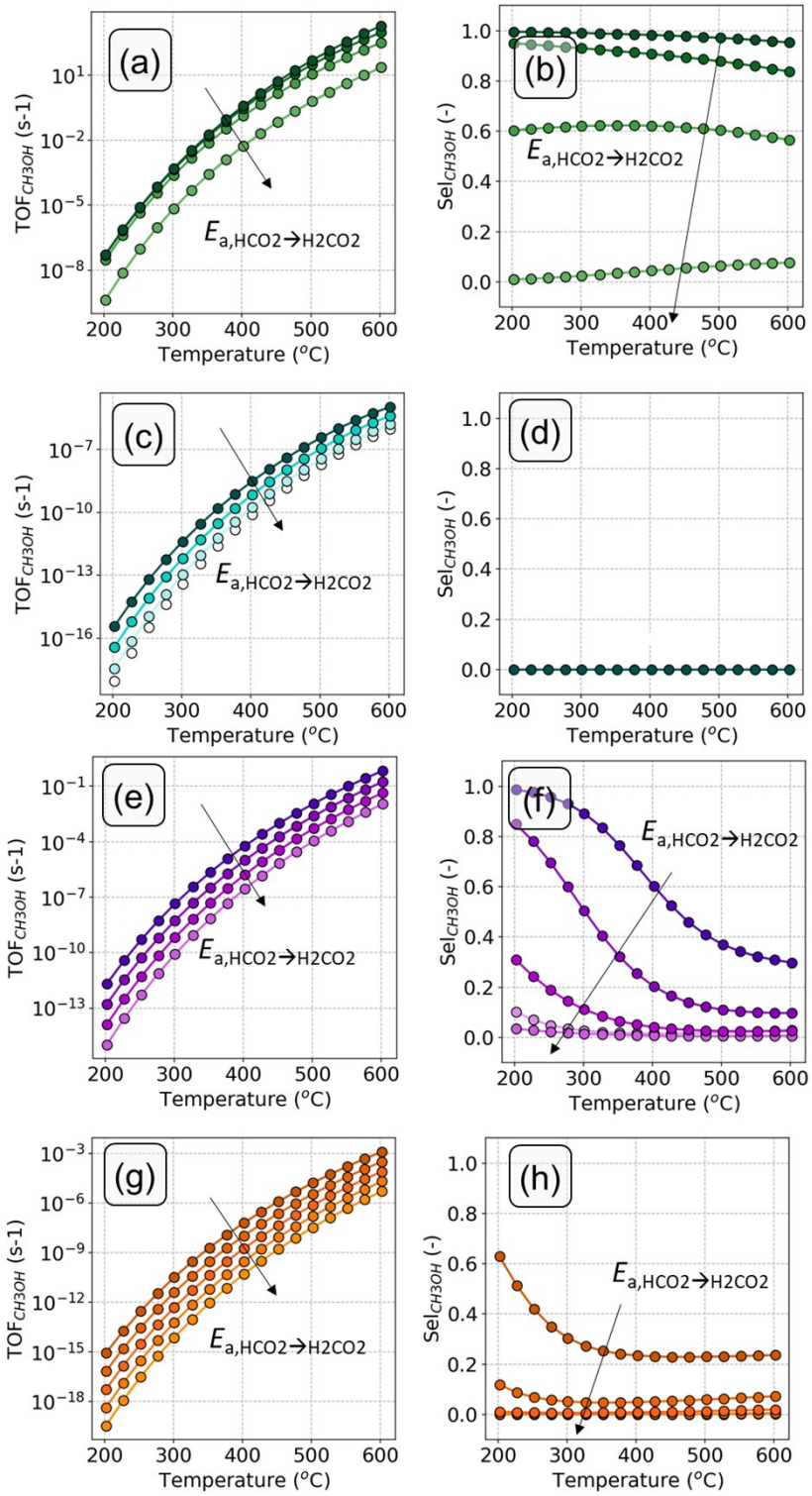

Fig. S8. Sensitivity of the microkinetic simulations at different values of the barrier of the step of HCO_2 hdyrogenation to H_2CO_2 (step 7). From light to dark the activation energy energy decreases by steps of 10 kJ/mol. (a-b) Ni-In_2O_3, (c-d) Pd-In_2O_3, (e-f) Pt-In_2O_3 and (g-h) Rh-In_2O_3.

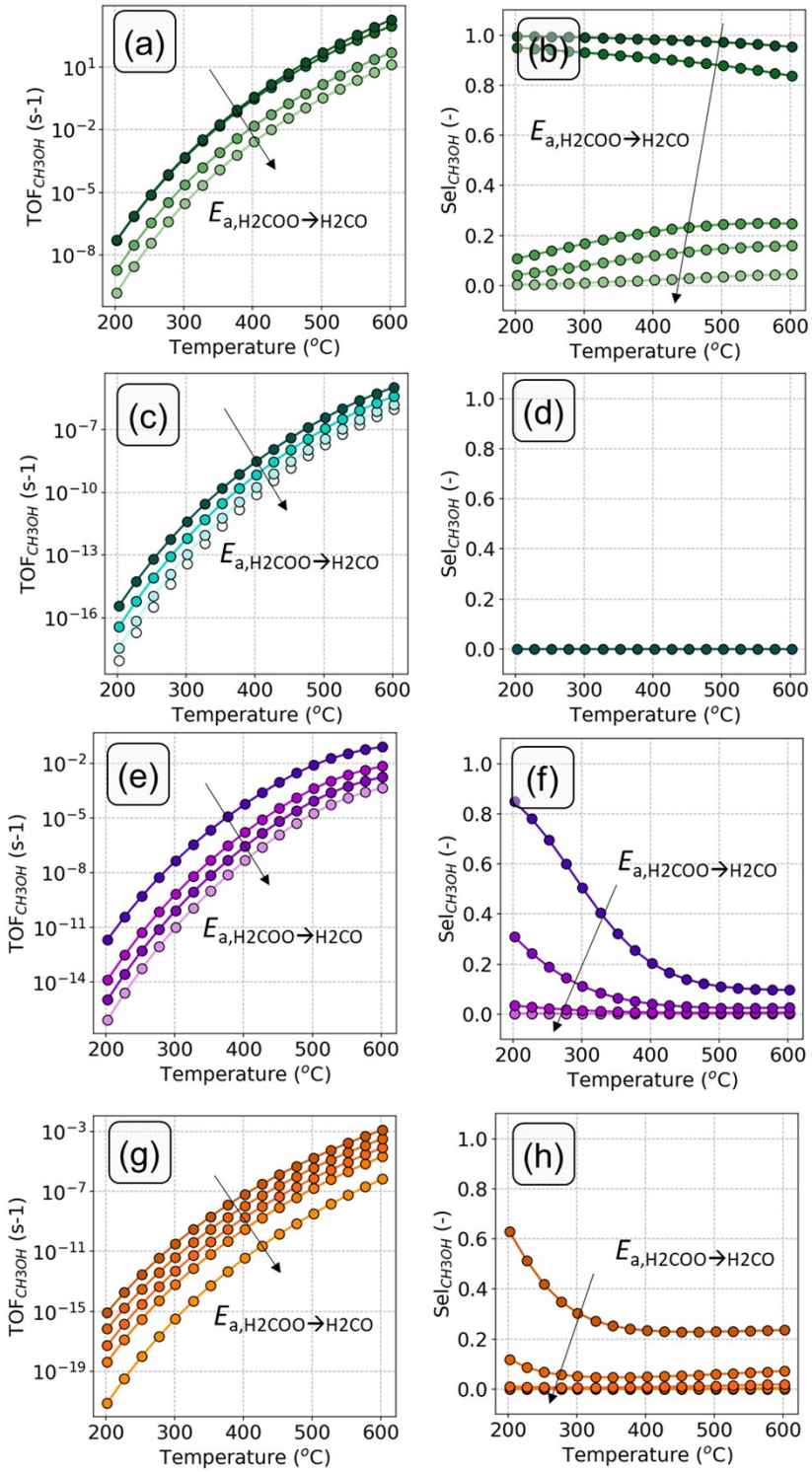

Fig. S9. Sensitivity of the microkinetic simulations at different values of the barrier of the step of H_2CO_2 hdyrogenation to CH_2O+O (step 8). From light to dark the activation energy energy decreases by steps of 10 kJ/mol. (a-b) Ni-In_2O_3, (c-d) Pd-In_2O_3, (e-f) Pt-In_2O_3 and (g-h) Rh-In_2O_3.

S10. Additional DFT Calculations

A fundamental assumption in this study was that each kinetic pathway exclusively employs a singular oxygen vacancy, in line with previous DFT calculations on In_2O_3. Although exploration of the full kinetic pathway involving a secondary vacancy is out of scope of this manuscript, we calculated a few key elementary steps. We calculated the step of HCOO hydrogenation to H_2COO on Pd-In_2O_3 as this step has the highest activation energy in the formate pathway to methanol. The results are reported in Tables S15-16. The presence of a second oxygen vacancy results in a lower barrier of 148 kJ/mol as opposed to the barrier of 220 kJ/mol found on Pd-In_2O_3 with one oxygen vacancy. Indeed, the hydrogenation from a Pd-H intermediate (Table S16) results in a lower barrier than the protonation from a O-H moiety as in the case with one Ov. However, this activation energy remians significantly higher than the main rate-limiting step (i.e. CO_2 dissociation; E_a = 65 kJ/mol). We can thus infer that the redox pathway remains dominant.

Table S15. Activation and reaction energies (kJ/mol) for the steps of HCOO hydrogenation on Pd-In_2O_3 with two oxygen vacancies.

	Elementary step	E_R	E_a
11	$HCOO^* + H^* \rightleftharpoons H_2COO^* + *$	86	148

Table S16. Structures of IS, TS and FS for the elementary reaction steps in Table S15.

$HCOO^* + H^* \rightleftharpoons H_2COO^* + *$		
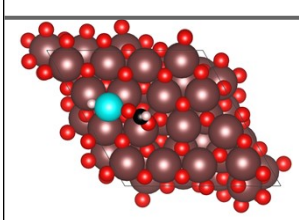	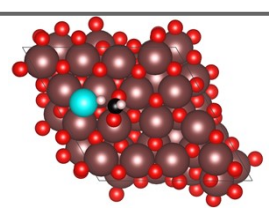	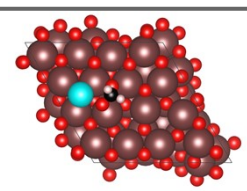

We also investigated the elementary steps of CO hydrogenatoion in the presence of an additional oxygen vacancy for Pt- and Rh-In_2O_3. The activation and reaction energies and structures are reported in Table S17-18. In the presence of a secondoxygen vacancy, the elementary steps of CO hydrogenation become accessible on Pt-In_2O_3. On Rh-In_2O_3, we still cannot find the TS for these elementary steps because the HCO intermediate is unstable on this model. The tables below show that the two hydrogenation steps on

Pt-In_2O_3 are associated with activation energies of 89 and 171 kJ/mol, respectively. The last step has an higher activation energy because it occurs via migration of an O-H to a Pt-H.

Table S17. Activation and reaction energies (kJ/mol) for the steps of CO hydrogenation on Pt-In_2O_3.

	Elementary step	E_R	E_{act}
14	$CO^* + 2H^* \rightleftharpoons HCO^* + H^*$	89	5
15	$HCO^* + H^* \rightleftharpoons CH_2O^* + *$	171	164

Table S18. Structures of IS, TS and FS for the elementary reaction steps in Table S17.

$CO^* + 2H^* \rightleftharpoons HCO^* + H^*$			$HCO^* + H^* \rightleftharpoons CH_2O^* + *$		
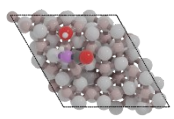	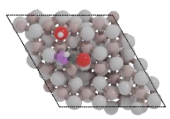	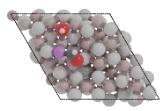	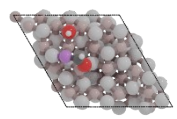	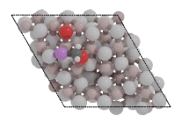	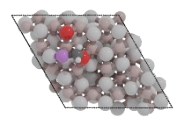

Supporting References

1 M. S. Frei, M. Capdevila-Cortada, R. García-Muelas, C. Mondelli, N. López, J. A. Stewart, D. Curulla Ferré and J. Pérez-Ramírez, *J. Catal.*, 2018, **361**, 313–321.

2 S. W. Benson, *J. Chem. Educ.*, 1965, **42**, 502–515.